THE ASTROPHYSICAL JOURNAL, 352:184–191, 1990 March 20

MAGNETIC FIELD AND SPATIAL STRUCTURE OF BIPOLAR OUTFLOW SOURCES

KLAUS-WERNER HODAPP
Institute for Astronomy, University of Hawaii
Received 1989 June 26; accepted 1989 September 16

ABSTRACT

Deep *K* band images of three bipolar outflow sources (Cep A, GL 490, and R Mon) are presented. The polarization of background or embedded stars close to these star-forming regions has been measured in the *I* band to determine the local projected magnetic field direction. For Cep A the outflow direction and the magnetic field are almost parallel as is the case for most bipolar outflow sources. This alignment is poorer in the case of R Mon while GL 490 is a peculiar case with the outflow direction almost perpendicular to the local magnetic field. No indication was found for a distortion of the magnetic field close to the collimating disks of the outflows.

Subject headings: infrared: sources — magnetic fields — nebulae: reflection — polarization

I. INTRODUCTION

Many young stellar objects show signs of mass outflow, such as high-velocity molecular gas, often with bipolar morphology, or shock excited emission in the form of Herbig-Haro (HH) objects or jet like optical emission regions. Most of these objects are highly polarized and, when spatially resolved, are associated with infrared reflection nebulae (e.g., Werner, Dinerstein, and Capps 1983; Lenzen, Hodapp, and Solf 1984, hereafter LHS).

In this class of objects, the CO-outflow direction tends to be aligned with the ambient magnetic field direction and to be perpendicular to the average infrared polarization angle of the object itself (Hodapp 1984). This is evidence for the formation of a disk perpendicular to the magnetic field lines that, when seen almost edge-on, obscures the central source, letting only scattered, highly polarized light reach the observer. Further, it indicates that the large-scale CO outflow is collimated by interaction with the disk or the magnetic field. These findings can be understood in hydromagnetic wind models (e.g., Pudritz and Norman 1986, and references therein), in which both the bipolar molecular flows and optical jets are produced in accretion disks and collimated by magnetic field lines threading those disks. While some star-forming regions seem to be controlled by well-ordered magnetic fields, and have good alignment between different outflows and the field (e.g., Moneti *et al.* 1984; Gomez de Castro, Eiroa, and Lenzen 1988), others, in particular regions of massive star formation, do not fit into this simple picture. Earlier studies of the relation between magnetic field orientation and outflow direction relied on polarization measurements of stars of relatively low extinction and therefore probed only the periphery of the star-forming molecular clouds. To study the magnetic field geometry close to the newly formed stars, it is necessary to measure the polarization of faint, heavily reddened stars that probe the magnetic field in the denser parts of a molecular cloud.

In this paper, the relation between the infrared reflection nebulae and the local magnetic field in three well-known infrared sources, Cep A, GL 490, and R Mon will be studied. Deep, high-resolution *K* band images of these objects were taken to study the infrared reflection nebulae associated with them. The motivation here is to find clues about the orientation of the molecular disk driving the bipolar mass outflow from either color gradients in the reflection nebula, indicating extinction variations, or from scattered light from the boundary region between the outflow and the ambient molecular cloud. The magnetic field geometry in the molecular cloud close to the posited disk around the central young star was probed by *I* band polarimetry of stars in the background of or embedded in the molecular cloud.

II. OBSERVATIONS AND DATA REDUCTION

a) I Band Polarimetry

The *I* band polarization measurements of background stars were done with a double calcite plate (Savart plate) on loan from the Max-Planck-Institut für Astronomie in Heidelberg. A RG 830 filter was used to define the bandpass of the observations, which was close, although not identical, to the *I* band. The detector was an 800×800 Texas Instrument CCD. The instrument was used at the f/10 focus of the University of Hawaii 2.2 m telescope.

The Savart-plate method for measuring the polarization of point sources (Röser 1981) is advantageous for this type of polarization survey, since it gives a polarization value for every pointlike object in the $\sim 2' \times 2'$ field of view of the detector. For the observations discussed here, the exposure time for individual frames was 300 s at each position of the Savart plate. Twelve such exposures with Savart plate orientations ϕ in steps of 30° were obtained at every position in the field surveyed. The images were dark-current subtracted and flat-fielded using incandescent light dome flats. The Savart-plate produces two orthogonally polarized images of every object in the field. The distance between the two images is constant, but their relative position angle changes with the orientation of the Savart plate, which can thereby be measured easily. Photometry on the double images was done with a circular aperture photometry program written by M. Buie. While doing the photometry, all the images were visually inspected, and all image pairs showing obvious problems, mostly image overlap and bad pixels, were discarded. As the result of these image-processing steps, the normalized intensity difference for each Savart plate orientation $(I_1 - I_2)/(I_1 + I_2)(\phi)$ was obtained for each star in the field. The set of 12 such normalized intensity differences was then fitted by a cosine law, giving the polarization p and the polarization angle Θ. The errors given for the polarization values are the rms residuals of the data from the

best fitted cosine function, divided by the root of the number of frames used.

In order to measure instrumental polarization effects, some stars of known polarization from the list of Mathewson and Ford (1970) and a field in Mon R2 with some faint stars of known polarization (Hodapp 1987) were observed. An instrumental polarization of 2.5%, most likely caused by polarization effects in the CCD detector itself, was found and corrected for in the data. The orientation of the CCD chip was measured using star trails obtained with the telescope tracking stopped and was taken into account when computing the polarization angles. In each star-forming region several partly overlapping fields were observed, covering the region where magnetic field distortions by a disklike structure could have been expected. For Cep A, six fields were observed, for GL 490 four, and for R Mon two.

b) *Infrared Imaging*

The UH Infrared Camera was used at the f/10 focus of the 2.2 m telescope to obtain deep images in the H band (1.65 μm) and K band (2.2 μm) of the infrared reflection nebulae associated with the newly formed stars in the regions studied. The Infrared Camera was equipped with a 128 × 128 HgCdTe detector array manufactured by Rockwell International and on loan to us from JPL's HIRIS project. This detector, which is optimized for the operating conditions of the HIRIS project, has a read noise of ~2000 electrons and a well capacity of 800,000 electrons, thus always being read-noise limited. At the operating temperature of 100 K, the device has a peak quantum efficiency of 30% in K, with variations of a factor of 2 across the chip.

The observations were done by taking alternate object and sky exposures. Between pairs of exposures, the telescope was moved by a few arcseconds. This allowed elimination of stars in the "sky"-position frames by computing a median of a number of such exposures taken close in time to the object exposure. The resulting median sky frame was subtracted from the object frame and the result was then flat-fielded using an incandescent light dome flat. The individual images were registered (0.5 pixel spacing), coadded, and normalized, eliminating bad pixels by using a bad pixel mask in the coaddition process. The halftone images (Figs. 1, 4, and 7; see § III) are scaled logarithmically to bring out low-level features while still retaining some information close to the bright and overexposed central star. In the case of Cep A, the standard stars HD 225023 and HD 203856 (Elias *et al.* 1982) were used to calibrate the frames photometrically in the H and K bands.

III. DISCUSSION

a) *Cep A*

Hodapp and Eiroa (1989) recently studied the Cep A region using high-resolution K band imaging and H band polarimetry of background stars. They found indications for a bent magnetic field, which they interpreted using the model of sequential star formation of Sargent (1977). In this paper, much deeper H and K band images are discussed in an attempt to elucidate the orientation and the extent of the collimating disk of the bipolar outflow. Also, I band polarization measurements of faint stars close to the outflow sources are used to better determine the magnetic field orientation close to the disk and the outflow.

The K band image (Fig. 1 [Pl. 3]) shows a number of unresolved sources in the region of the posited dense dust disk to the southwest of the main reflection nebula, in particular a group of three point sources lying on the extension of the long axis of the reflection nebula IRS 6. These sources were undetected in the H band, and appear as pronounced peaks on the color map (Fig. 2). They were detected as a region of extended K band flux on the earlier, low-resolution maps of LHS, but have not been recognized as individual point sources. The positions of the three point sources in Figure 1 have been measured relative to three stars (4, 6, and 7 in Fig. 1) visible on the Palomar Observatory Sky Survey (POSS) red plate, which in turn have been measured relative to a number of SAO stars. These positions have estimated errors of 2″ in both coordinates. Star 4, which is IRS 5 in LHS, was measured to be $0^s.35$ (2″.5) west of the position given by LHS. The three very red stars in the group of point sources west of the reflection nebula have coordinates in equinox 1950.0: $22^h54^m17^s.3$, 61°45′47″; $22^h54^m17^s.6$, 61°45′45″; and $22^h54^m17^s.7$, 61°45′48″. About 10″ north of this group of stars, there are two other heavily reddened point sources visible in Figure 1 (located at $22^h54^m17^s.7$, 61°46′01″ and $22^h54^m18^s.2$, 61°45′57″) which also might be embedded sources in the area of the dust disk. None of these point sources coincide in position with the unresolved radio continuum sources found by Hughes (1988) or with the illuminating source of the reflection nebula IRS 6 located by polarimetric observations (LHS). These K band point sources most likely are stars embedded in the Cep A molecular cloud, as suggested by the low-level extended flux surrounding the group of three sources. However, they are not the stars illuminating the reflection nebula and most likely are not the outflow source. It is conceivable that the central source of the outflows is in fact one of Hughes's (1988) radio sources and that this central source is so heavily obscured that it has not been detected at the sensitivity level reached in Figure 1, a hypothesis that could be tested by deep L band imaging.

The K/H color map (Fig. 2) shows a similarly steep increase in reddening toward the southwestern edge of the reflection nebula as the L/K map of LHS. The extinction-defined southwestern edge of the reflection nebula has in general a conical shape that resembles those of other IR-reflection nebulae (e.g., Hodapp *et al.* 1988). The reddening in the flux minimum at the southern edge is particularly strong. This minimum seems to be a local extinction enhancement and indicates that the extinction by the disk is patchy on a scale of ~1000 AU, assuming the distance to Cep A to be 730 pc (Blaauw, Hiltner, and Johnson 1959). The northern edge of the reflection nebula is also very red, while the rest of the reflection nebula is more uniform in color, a result that was already indicated, although less pronounced, on the L/K map of LHS.

Besides the point sources already discussed above, a number of other highly reddened point sources are visible in Figure 2. These are either embedded stars or background stars shining through the densest part of the disk. In the K band image (Fig. 1) three stars are identified by their numbers in Figure 3 and Table 1. Note that in Figure 3 the (unnumbered) star southwest of star 6, which is brighter than star 6 in K, is fainter than star 6 in H (Fig. 2) and is invisible in the I band. It must therefore be heavily obscured. Similarly, it is interesting to note that the star on the western edge of Figure 1, located approximately midway between stars 3 and 4, is invisible in the I band (Fig. 3). This, together with the nondetection in the H band of the group of three faint point sources discussed earlier, gives an idea about the extension and density of the dust disk in Cep A.

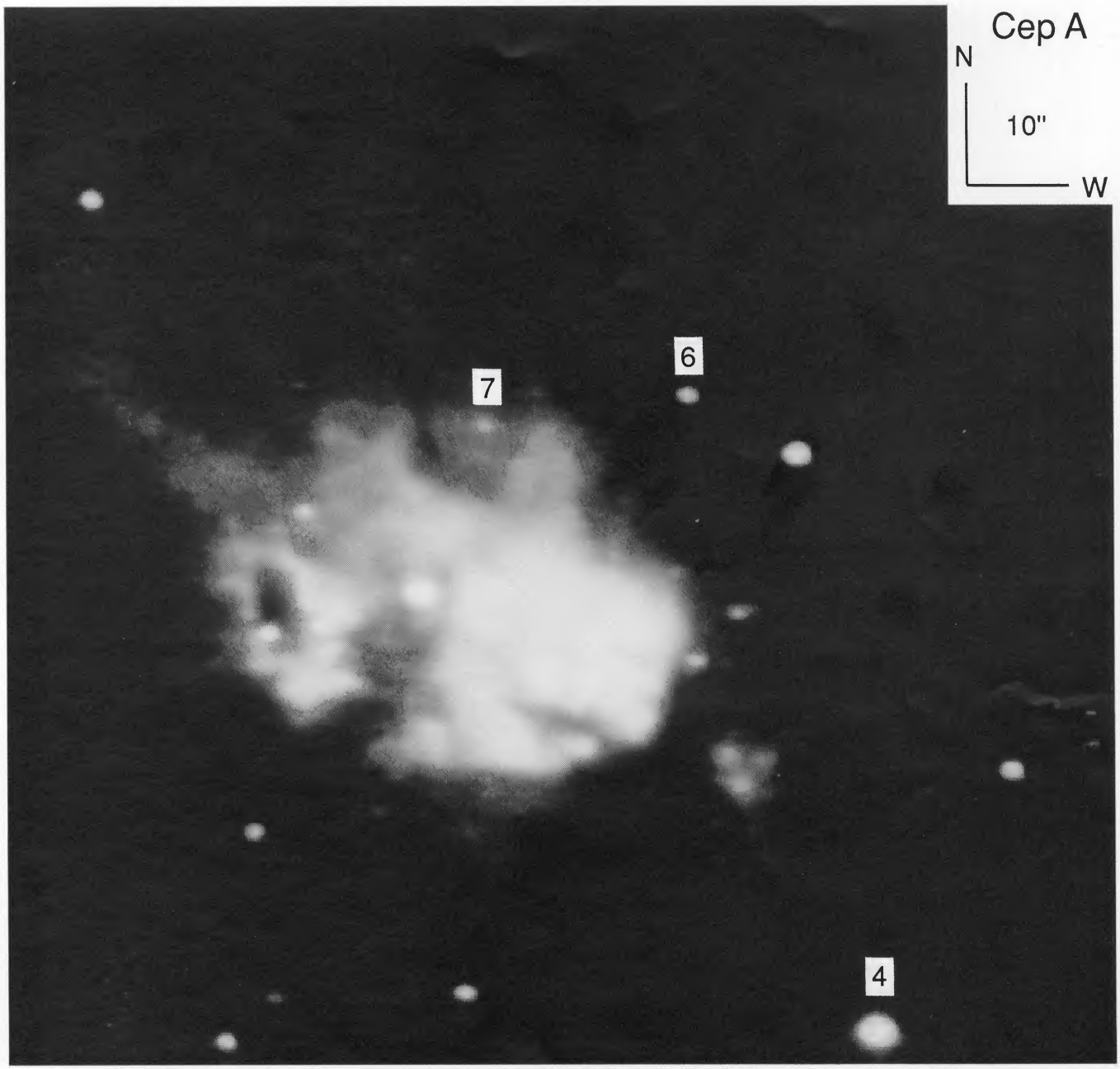

FIG. 1.—*K* band image of the Cep A star-forming region. Some stars are identified by their number in Fig. 3 and Table 1.

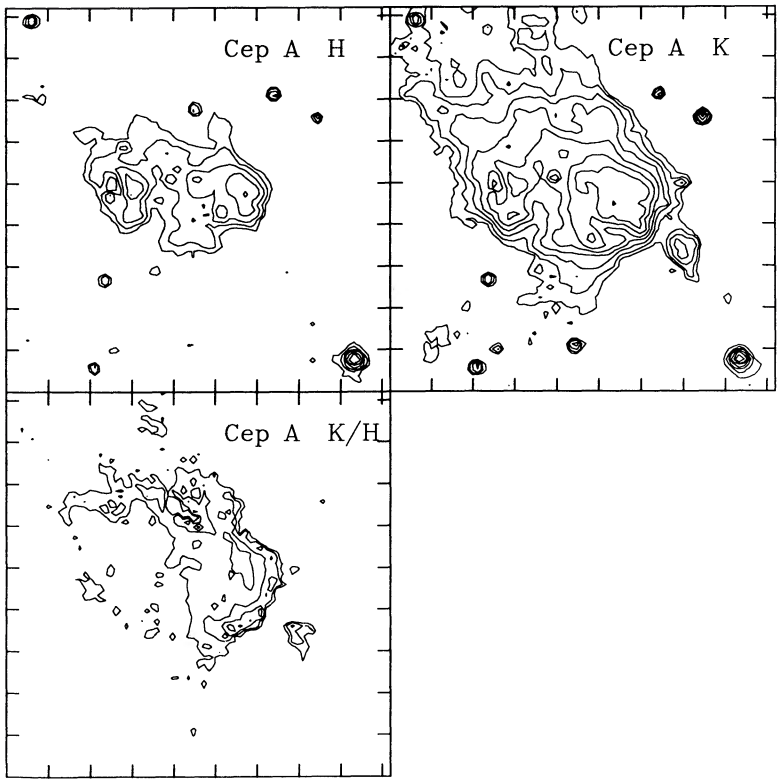

FIG. 2.—Contour plots of Cep A in the K and H bands and a K/H color map. In the H and K maps, the contours are 100, 200, 400, ... μJy/arcsec^{-2}. The contours in the K/H map are flux ratios of 10, 20, 40, and 80. The bright source in the southwest corner of the H band and K band maps is star 4 (LHS IRS 5), its coordinates are $22^h54^m15^s.74 + 61°45'21''.7$ (1950.0).

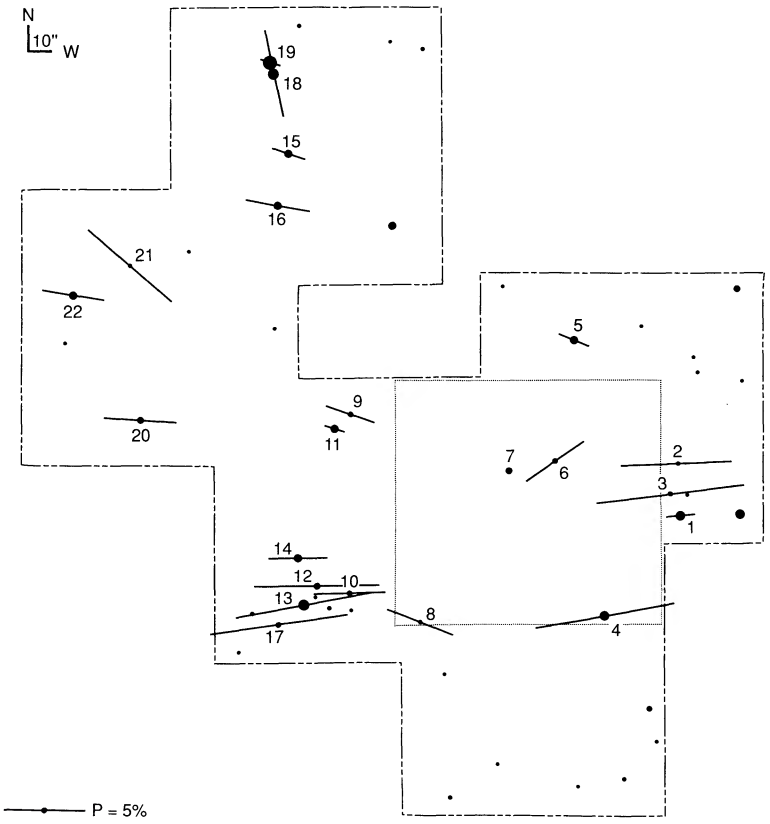

FIG. 3.—Background star polarization map of Cep A in the I band. The size of the points in this map symbolizes I magnitudes. The dotted line indicates the area of the K band image (Fig. 1).

TABLE 1

I BAND POLARIZATION OF STARS NEAR CEP A

Star	p (%)	Θ
1.....	1.8 ± 0.5	$95° \pm 8$
2.....	6.8 ± 1.0	92 ± 4
3.....	9.1 ± 2.2	97 ± 7
4.....	8.6 ± 0.7	100 ± 2
5.....	$2.0 \pm 0.,1$	67 ± 2
6.....	4.3 ± 0.3	125 ± 2
7.....	unpolarized	...
8.....	4.4 ± 0.8	69 ± 5
9.....	3.2 ± 0.7	71 ± 6
10.....	4.5 ± 0.6	91 ± 4
11.....	1.3 ± 0.3	72 ± 7
12.....	7.7 ± 0.4	90 ± 2
13.....	8.4 ± 0.6	100 ± 2
14.....	3.6 ± 0.7	91 ± 6
15.....	2.1 ± 0.2	71 ± 3
16.....	4.1 ± 0.3	80 ± 2
17.....	8.5 ± 0.5	98 ± 2
18.....	5.4 ± 0.2	12 ± 1
19.....	1.3 ± 0.2	71 ± 5
20.....	4.5 ± 1.0	86 ± 7
21.....	6.8 ± 0.8	49 ± 4
22.....	3.9 ± 0.2	81 ± 2

Those stars that appear as point sources in the color map (Fig. 2) have K/H flux ratios of 10 or more. Assuming $H-K = 0.1$ A_V (e.g., Mathis, Mezger, and Panagia 1983), this corresponds to at least $A_V = 27$ mag, even if the background stars are assumed to be late M stars. This lower limit adds to the evidence for a large, dense disk enshrouding the active star-forming region in Cep A.

Only two of the stars with polarization measurements in Table 1 had been measured previously. Star 4 is identical to Hodapp and Eiroa's star 16 ($\Theta = 107°$ in their paper) and to LHS's IRS 5, which is the bright point source in the lower right of Figure 1. Stars 18 and 19 in this paper were unresolved on POSS plates and appear as star 19 on Hodapp and Eiroa's list. It is not clear which of the two stars dominated the *H* band measurement, but it is certain that star 18, with its polarization angle of 12°, is responsible for the peculiar polarization value at this position in the *H* band.

The polarization vectors of background stars seem to define two spatially separate groups of stars. The close pair of stars 18 and 19 will be excluded from this discussion since systematic errors in the polarization due to image overlap are likely to affect these two stars. The first group of stars is lying west and south of the infrared reflection nebula and encompasses it. The average polarization angle in this group which includes stars 1, 2, 3, 4, 5, 6, 8, 10, 12, 13, 14, and 17, is $\Theta = 92\overset{\circ}{.}9$ with a standard deviation of the mean value of $\sigma = 4\overset{\circ}{.}5$. The second group comprises all stars lying in the direction of the outflow to the northeast of the reflection nebula, i.e., stars 9, 11, 15, 16, 20, 21, and 22. The average polarization angle in this second group of stars is $\Theta = 72\overset{\circ}{.}9$ with a standard deviation of the mean value of $\sigma = 4\overset{\circ}{.}9$. Purely from a statistical point of view, the difference in the polarization angles is marginally significant. The separation of the stars into the two groups is somewhat arbitrary. Star 5, in particular, might be included in the second group instead, since it is now by far the northernmost member of the first group. This would make the distinction between the two groups more significant. The existence of two spatially separated groups of stars with distinct polarization properties can be explained by either a local distortion of the magnetic field (Hodapp and Eiroa 1989) or by the superposition of two cloud filaments with different magnetic field orientations and consequently with different polarization effects. Even though the data presented here sample the projected magnetic field much better than Hodapp and Eiroa's *H* band data, they still do not allow a decision between these two models.

As discussed above the extinction to the south west of Cep A IRS 6 shows some complex structure (Figs. 1 and 2). A simple model describing the color variations as due to a disk viewed edge-on would place the normal of this disk at a position angle of 45°. This agrees with the disk orientation derived from the low-velocity CO feature measured by Hayashi, Hasegawa, and Kaifu (1988). High-velocity CO features, on the other hand, define an outflow axis at 90°, parallel to the local magnetic field direction. Optical signposts of outflow activity are aligned at an intermediate angle of 70°, which is also the orientation of the long axis of the reflection nebula IRS 6. As discussed by Hayashi, Hasegawa, and Kaifu (1988), the outflow phenomena in Cep A cannot be explained by a simple bipolar outflow model.

b) GL 490

The *K* band image of GL 490 (Fig. 4 [Pl. 4]) shows an arclike feature extending to the south of the central source and then bending toward the southwest. Extended emission is also seen west of the bright point source. The general structure of the extended emission in Figure 4 agrees well with the map at lower spatial resolution but higher sensitivity by Yamashita *et al.* (1989). From their polarimetric measurements, it is clear that the extended emission is a reflection nebula illuminated by the central star. The reflection nebula appears parabolic, similar to other reflection nebulae associated with bipolar outflow objects. Its symmetry axis is pointing to the southwest, the same direction as the *I* band structure seen by Campbell, Persson, and McGregor (1986, hereafter CPM), and the CO-outflow direction as measured by Snell *et al.* (1984) which both define an outflow axis at $\sim 45°$. The "arc" seen in Figure 4 is the eastern and southern boundary of the parabolic reflection nebula. As discussed by Yamashita *et al.* (1989) for GL 490 and R Mon, and similar to the case of L1551 IRS 5 (Mundt and Fried 1983; Campbell *et al.* 1988), the parabola-shaped reflection nebula results from scattered light in an optically thin region of enhanced dust density that marks the boundary between the "nozzle" of the outflow and the ambient molecular cloud material. The shape of the outflow region defined by this "arc" south and west of GL 490 and the reflection nebulosity directly west of the central source is very similar to the structure seen in the 2 cm VLA map of CPM on a much smaller spatial scale. The stellar objects E1 and E2 as labeled by CPM are clearly visible on the image (E2 lies within the eastern diffraction spike of the central source). Their source W is also visible in Figure 4, $\sim 14''$ west of the central source. The region labeled "Jet" in their Figure 1*c* contains another point-like object, between the central source and W, and extended emission north and south of it. The "arc" seen in the *K* band images has no corresponding feature in the optical. However, assuming that this "arc" is parabola shaped and extrapolating from the region imaged in Figure 4 it is obvious that all the *I* band extended emission lies within this parabola. This is similar to the situation in L1551 IRS 5 (Hodapp *et al.* 1988) and confirms that the "arc" is the density enhanced but optically thin boundary region between the outflow and the

PLATE 4

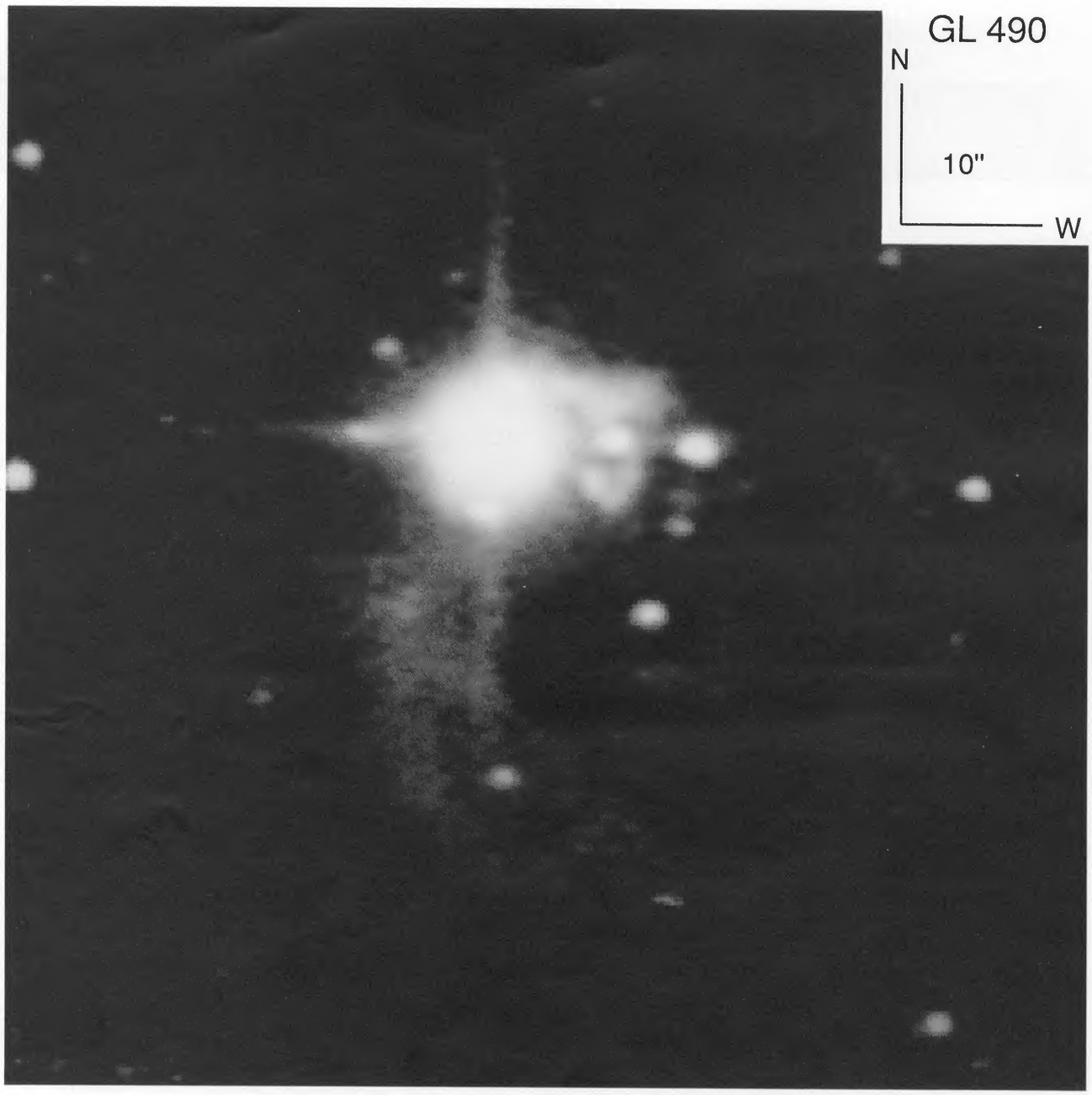

FIG. 4.—*K* band image of GL 490

ambient molecular cloud. Outside of this boundary, in particular southeast of it, lies a region of high extinction, very likely a dense part of the parent cloud of GL 490.

CPM have proposed a model for GL 490 that posits that the optical counterpart of GL 490 is purely scattered light from a polar lobe of a bipolar structure. They predict that the optical image of GL 490 be extended and displaced from the true position of the central star. Since the true nature of the optical and near-infrared counterpart of GL 490 is of fundamental importance to our understanding of this object, this problem will now be discussed again in light of the new data presented here. It is clear from the *K* band image (Fig. 4) and from the polarization measurements of Yamashita *et al.* (1989) that GL 490 is surrounded by reflection nebulosity that in any finite aperture contributes to the polarization of the central source. Despite that, the observations seem to support a model where the optical image of GL 490 is direct light from its central star and where the polarization arises predominantly from selective extinction by aligned grains.

CPM measured the source size and shape of GL 490 on their *R*-band and *I*-band images and on Maximum Entropy deconvolutions of these images. They claimed that GL 490 is extended and of cusplike shape, which they interpreted as evidence that the optical counterpart of GL 490 is almost entirely scattered light. The *K* band image in Figure 4 has a higher spatial resolution than their images, and a contour plot of the same data set (Fig. 5) clearly shows that there are two unresolved sources close to GL 490, most likely stars associated with it. One of these stars lies directly south of the central source and the other north at about a position angle of $-10°$. These two point sources blended into the image of the central source to produce the apparent extension in CPM's image. The central source in our image does not show any signs of being extended, as far as can be seen from the saturated image in Figure 5.

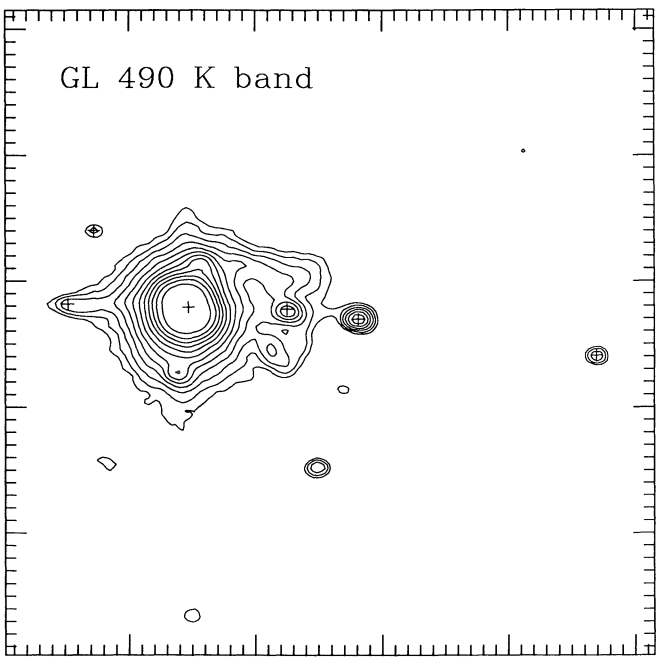

FIG. 5.—Contour plot of the *K* band image of GL 490 with *I* band positions included (*plus signs*). Small tick marks are 1′. The data are not calibrated photometrically. The contour levels are spaced in $2^{1/2}$ intervals in flux.

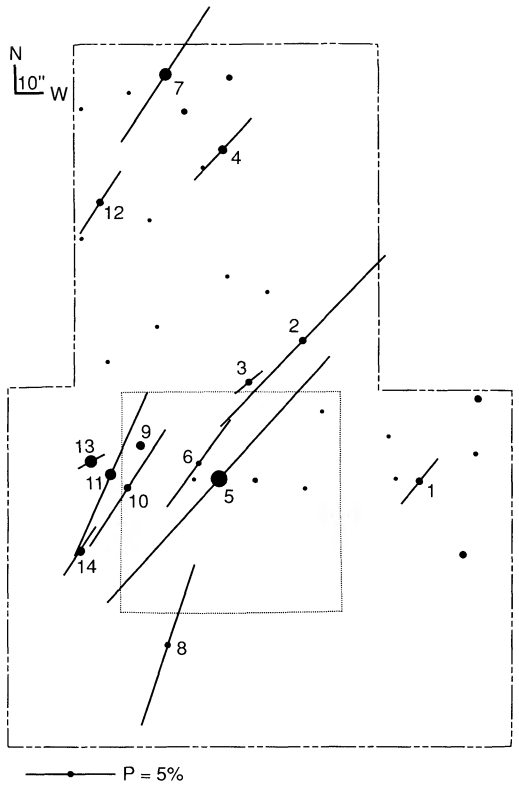

FIG. 6.—Background star polarization map of GL 490 in the *I* band. The size of the points in this map symbolizes *I* magnitudes. The dotted line indicates the area of the *K* band image (Fig. 4).

The positions of stars close to GL 490, including the position of its optical counterpart (star 5 in Fig. 6), were measured on the Savart-plate *I* band frames. By transforming the image scale, shifting, and rotating the image, the positions of the stars were fitted onto the *K* band image in Figure 5. The measured *I* band position of GL 490 lies less than 0.″2 away from the center of the contours of the saturated *K* band image of this source. Thus, in the wavelength range from *I* band to *K* band, there is no indication for a shift in the position of GL 490's central source with wavelength relative to neighboring stars. CPM's pure scattering model would predict a shift of the position of the flux maximum with wavelength and such a shift has indeed been observed in the case of L1551 IRS 5, from which only scattered light reaches the observer at optical and near-infrared wavelengths (Campbell *et al.* 1988; Hodapp *et al.* 1988).

The displacement of the 2 cm flux maximum from the optical position of GL 490 discussed by CPM does not necessarily imply that the optical image is displaced from the position of the central star. As discussed by Massi, Felli, and Simon (1985; see their Fig. 5) for the "blister" H II region associated with Mon R2 IRS 1, a compact H II region ionized by a star not located in its center has its radiocontinuum flux maximum offset from the ionizing star and has flux contours closely resembling CPM's 2 cm map.

The *K* band observations of a polarized reflection nebula illuminated by GL 490 by Yamashita *et al.* (1989) compared with the *I* band polarization data of point sources near GL 490 (Fig. 6 and Table 2) show that these point sources are not just compact condensations in the reflection nebula, but rather stars, polarized not by scattering but by selective extinction by

TABLE 2

I BAND POLARIZATION OF STARS NEAR GL 490

Star	p (%)	Θ
1.....	3.3 ± 0.4	141° ± 4°
2.....	13.3 ± 0.6	136 ± 2
3.....	2.0 ± 0.5	130 ± 7
4.....	4.7 ± 0.3	137 ± 2
5.....	18.6 ± 0.4	138 ± 1
6.....	6.1 ± 1.8	144 ± 9
7.....	8.9 ± 0.9	147 ± 3
8.....	9.5 ± 1.3	159 ± 2
9.....	unpolarized	...
10.....	7.7 ± 1.4	147 ± 5
11.....	10.0 ± 0.3	156 ± 1
12.....	4.2 ± 0.3	147 ± 2
13.....	1.7 ± 0.2	119 ± 4
14.....	3.3 ± 0.2	146 ± 2

aligned grains. The polarization angle of GL 490 (star 5), is very similar to that of other stars in the field, as expected if it is also polarized by aligned grains in the surrounding molecular cloud. In a scattering model, this alignment of the polarization of GL 490 with that of neighboring stars would be coincidental. The wavelength dependence of polarization of GL 490 (Hodapp 1984) does not allow a clear distinction between the two models discussed here. A simple, pure scattering model would predict the polarization to be wavelength independent, similar to what is actually observed in L1551 IRS 5 (Nagata, Sato, and Kobayashi 1983). The polarization in GL 490 decreases with wavelength (Hodapp 1984) but cannot be fitted well with a Serkowski-type law derived from the wavelength dependence of interstellar polarization.

Summarizing the above discussion, there is strong evidence that the optical and near-infrared image of GL 490 is direct light from its central young star and that the polarization arises from selective extinction by aligned grains in the molecular cloud surrounding GL 490.

GL 490 is one of the few exceptions from the general rule that the outflow axes of bipolar sources tend to be parallel to the projected local magnetic field direction; other exceptions are HH 12 and DG Tau (Heyer, Strom, and Strom 1987). In GL 490, the outflow axis is almost perpendicular to the magnetic field direction, as indicated by the polarization of background stars. One possible explanation for this is that the polarization arises in foreground or background clouds unrelated to GL 490. On the POSS prints, the molecular cloud complex containing GL 490 is well defined, and there is no indication for substantial extinction unrelated to this cloud along the line of sight. Further, the large-scale magnetic fields direction in the area around GL 490 (Hiltner 1956; Kobayashi *et al.* 1978) is the same as that measured close to GL 490, indicating that the molecular cloud magnetic field is well aligned with the interstellar field. It is therefore very likely that the polarization direction of field stars around GL 490 marks the projected magnetic field direction in GL 490's parent molecular cloud. This implies that the bipolar mass outflow in GL 490 and the disk collimating it are decoupled from the local magnetic field or that the magnetic field in the area of the collimating disk is decoupled from that in the rest of the molecular cloud.

Finally, it should be noted that the density of faint stars within a radius of 20″ (0.1 pc at a distance of 1 kpc; Snell *et al.* 1984) seems larger than in other parts of the field (Fig. 4). With the small number of stars found and the small area covered by Figure 4, this result can only be tentative and needs confirmation by deeper images covering a larger area. The higher stellar density close to GL 490 can be interpreted as a small group of stars with GL 490 being its most luminous member.

In an attempt to explain the alignment of most outflow sources with the local magnetic field and the existence of a small number of outflows seemingly not aligned with the magnetic field, Heyer, Strom, and Strom (1987) noted that differences in the degree of ionization of the molecular clouds would affect the coupling of cores to the magnetic field. If GL 490 has formed as the most luminous member of a small group of stars, the ionization levels in its parent molecular cloud should have been fairly high, leading to strong coupling with the magnetic field. This contradicts the observed misalignment of GL 490's outflow with the local magnetic field. A plausible explanation for the orientation of the outflow associated with GL 490 is that some of the lower luminosity stars in the cluster underwent an outflow phase prior to the formation of GL 490, which by creating turbulence within the molecular cloud core destroyed the alignment with the magnetic field.

c) R Mon

The variable star R Mon (Schmidt 1861) is associated with the cometary reflection nebula NGC 2261, which is changing its appearance on time scales as short as a few months (Hubble 1916; Duncan 1956). R Mon is embedded in a disk-shaped molecular cloud and is the source of a bipolar outflow, according to CO measurements made by Cantó *et al.* (1981). In their model, the Herbig-Haro object HH 39 (Herbig 1968) is shock-excited emission produced when the blueshifted northern outflow lobe hits a small molecular cloud lying in its way. The *K* band morphology of R Mon/NGC 2261 is different from that at visible wavelengths. The eastern edge of NGC 2261 is most prominent in *K*, while the rest of the reflection nebula is very faint. The *K* band map of Yamashita *et al.* (1989) shows a more symmetric structure of the reflection nebula. The difference in the appearance of the outflow region is caused by the sharpness of the flux ridge in the eastern part of the nebula. The high surface brightness makes this region look more prominent in Figure 7 (Plate 5) than on the lower resolution map of Yamashita *et al.* Aspin, McLean, and Rayner (1987) have published *J* band and narrow-band *L* images of the same object. In *J*, the eastern part of NGC 2261 is brighter than the rest of the nebula, quite similar to the *K* band image presented here. The narrow-band *L* image, on the other hand, shows a jetlike feature extending directly east from the central star. On the *K* image (Fig. 7), this feature would coincide with the eastern diffraction spike, so it is not possible to draw any conclusions about it from our image. Similar to the case of GL 490, the parabola-shaped feature is interpreted as the inner wall of the cavity or nozzle blown free by the outflow, which agrees with the findings of Cantó *et al.* (1981). It should be noted that the inner parts of the parabola feature are approximately parallel to the plane of the molecular disk, which Cantó *et al.* find to lie at position angles between 46° (their Fig. 2, v_{LSR} = 9.4 km s^{-1}) and 73° (their Fig. 5, v_{LSR} = 10.5 km s^{-1}). The rotation of the polarization angle at the position of the central source in R Mon observed by Jones and Dyck (1978) can be readily explained by the growing dominance of the eastern edge of the reflection nebula with wavelength, increasing the polarization angle with wavelength.

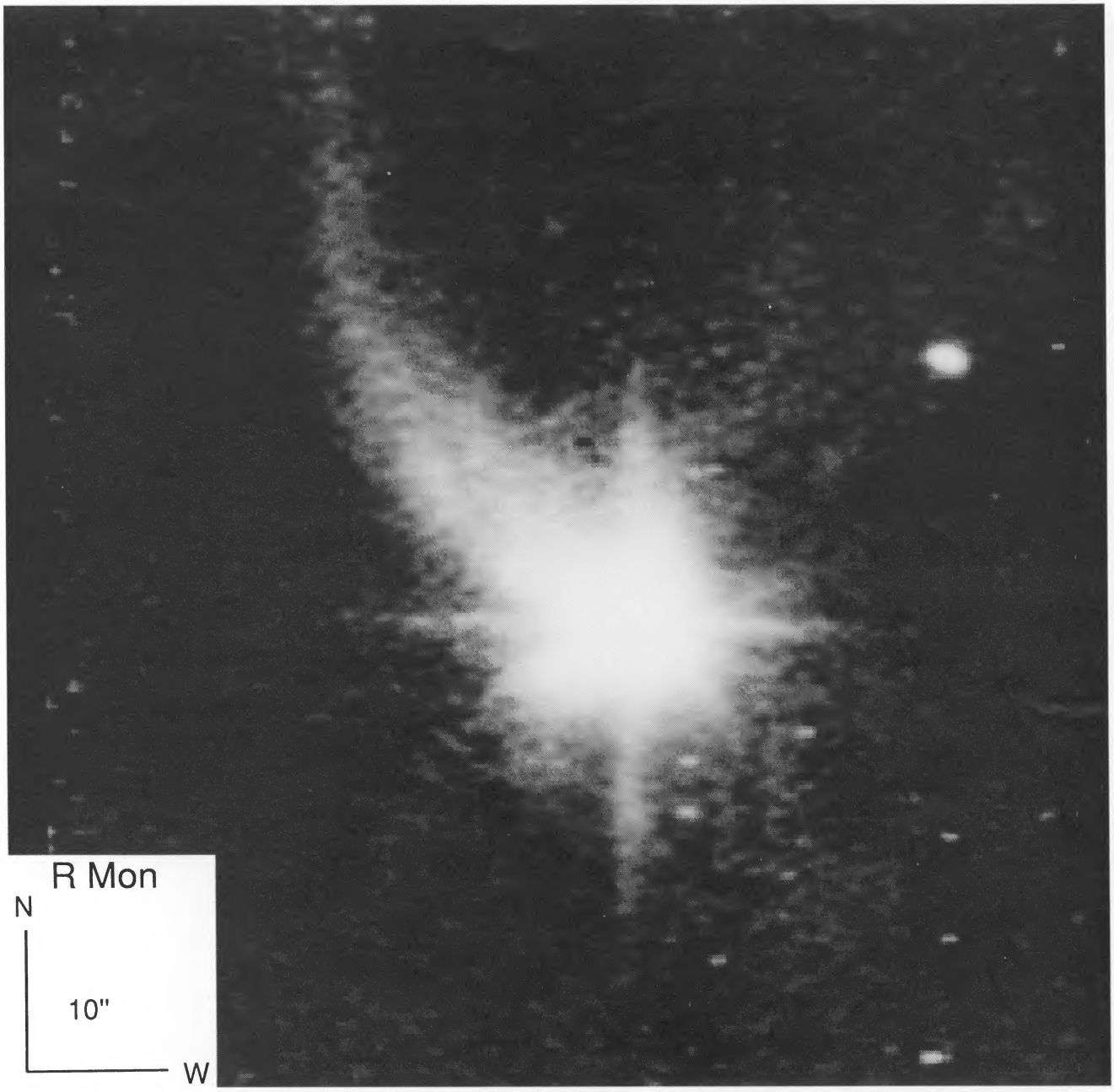

FIG. 7.—*K* band halftone image of R Mon

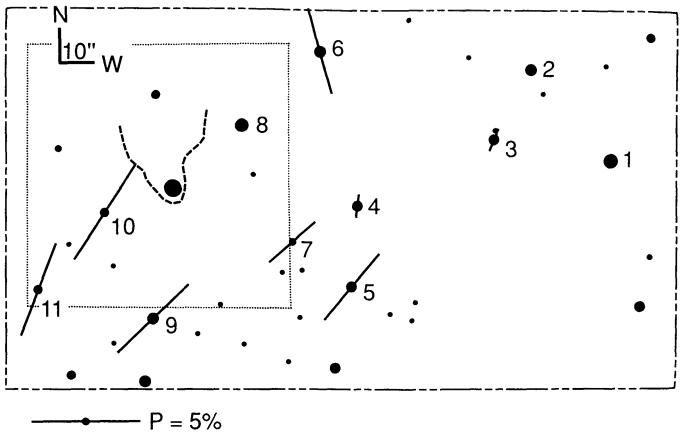

FIG. 8.—Background star polarization map of R Mon in the *I* band. The size of the points in this map symbolizes *I* magnitude. The dotted line indicates the area of the *K* band image (Fig. 7).

Polarization angles of stars (Fig. 8 and Table 3) in the region of the disk lie between 131° (star 7) and 159° (star 11) with the exception of star 6. Within the uncertainties of the disk orientation, the disk thus seems to be oriented perpendicularly to the projected magnetic field direction, which is the orientation expected from the collapse of a molecular cloud along the local magnetic field lines. From the map of the high-velocity CO components (Cantó *et al.* 1981, their Fig. 4) the outflow axis lies between position angles 0° (highest contours) and −7° (lowest contours), which agrees well with the position angle of HH 39 relative to R Mon. It can be concluded that in the case of R Mon, the alignment between the outflow axis and the local magnetic field direction is fairly poor.

TABLE 3

I BAND POLARIZATION OF STARS NEAR R MON

Star	*p* (%)	Θ	Number in Strom *et al.* 1986
1.....	unpolarized	...	20
2.....	unpolarized	...	26
3.....	1.1 ± 0.5	157° ± 13°	28
4.....	1.1 ± 0.7	173 ± 18	36
5.....	3.9 ± 0.5	140 ± 4	38
6.....	4.1 ± 1.0	16 ± 7	43
7.....	2.9 ± 0.7	131 ± 7	...
8.....	unpolarized	...	50
9.....	4.6 ± 0.4	137 ± 3	61
10.....	5.3 ± 1.4	148 ± 8	66
11.....	4.6 ± 1.5	159 ± 9	73

IV. CONCLUSIONS

The deep *K* band images and the *I* band polarimetry of stars presented in this paper lead to the following conclusions:

1. In Cep A the outflow direction and long axis of the reflection nebula are almost parallel to the local magnetic field. The disk, as far as its orientation can be determined from the available data, does not seem to be perpendicular to the magnetic field. The polarization data suggest that two groups of stars with distinct polarization properties exist close to Cep A. This might be caused by a superposition of two molecular filaments with different magnetic field orientations or might indicate a distorted structure of the magnetic field.

2. The *I* band counterpart of GL 490 was shown to be the central star of the bipolar mass outflow seen in direct light. Disk orientation and outflow direction in GL 490 do not show the usual relation to the magnetic field direction. The polarization of the central source and that of other stars in the field are parallel; the outflow axis is almost perpendicular to the magnetic field. There are indications that GL 490 is the most luminous member of a small group of stars.

3. The morphology of NGC 2261, the reflection nebula associated with R Mon, is different in the *K* band than at visual wavelengths. The flattened molecular disk surrounding R Mon is almost perpendicular to the magnetic field, while the outflow axis differs considerably from the magnetic field direction.

4. In none of the three cases studied here does the polarization pattern show the distortions expected from disk formation in a magnetized cloud (e.g., Dorfi 1982; Pudritz and Norman 1986; Kaburaki and Itoh 1987). With the still only sparsely sampled polarization data presented here, it is possible that the polarization pattern has not been sampled completely enough to show the predicted effect. However, in two other objects with well-studied magnetic field geometry, HH 7-11 and HH 33/40 (Heyer, Strom, and Strom 1987), the polarization pattern of background stars appears undisturbed in the same way as for the objects studied on this paper. It is therefore more likely that the nondetection of any magnetic field distortion pattern has more fundamental reasons. A possible explanation is that the grains in molecular disks around young stars lose their alignment with the magnetic field as a result of high gas densities, higher grain temperatures, and grain growth. It should be noted in this context that the mechanism for coupling the solid component of a molecular cloud to the magnetic field is friction (collisions) with its ionized component, which tends to destroy grain alignment. The observed undistorted polarization pattern might then be produced by grains in the outer parts of the molecular cloud, where grain alignment is maintained and the magnetic field is not noticeably distorted.

I thank H.-J. Röser for making the Savart plate available for the observations reported here. The HIRIS Infrared Array is the result of work by the JPL Infrared Technology Group under funding by the NASA Office of Space Sciences and Applications. Optical CCD development at the IFA has been partly supported by NSF grants AST 85-14575 and AST 86-15631.

REFERENCES

Aspin, C., McLean, I. S., and Rayner, J. T. 1987, in *Infrared Astronomy with Arrays*. ed. C. G. Wynn-Williams and E. E. Becklin (Honolulu: Institute for Astronomy, University of Hawaii), p. 281.
Blaauw, A., Hiltner, W. A., and Johnson, H. L. 1959, *Ap. J.*, **130**, 69.
Campbell, B., Persson, S. E., and McGregor, P. J. 1986, *Ap. J.*, **305**, 336 (CPM).
Campbell, B., Persson, S. E., Strom, S. E., and Grasdalen, G. L. 1988, *A.J.*, **95**, 1173.
Cantó, J., Rodriguez, L. F., Barral, J. F., and Carral, P. 1981, *Ap. J.*, **244**, 102.
Dorfi, E. 1982, *Astr. Ap.*, **114**, 151.
Duncan, J. C. 1956, *Pub. A.S.P.*, **68**, 517.
Elias, J. H., Frogel, J. A., Matthews, K., and Neugebauer, G. 1982, *A.J.*, **87**, 1029.
Gomez de Castro, A. I., Eiroa, C., and Lenzen, R. 1988, *Astr. Ap.*, **201**, 299.
Hayashi, S. S., Hasegawa, T., and Kaifu, N. 1988, *Ap. J.*, **332**, 354.
Herbig, G. H. 1968, *Ap. J.*, **152**, 439.
Heyer, M. H., Strom, S. E., and Strom, K. M. 1987, *A.J.*, **94**, 1653.

Hiltner, W. A. 1956, *Ap. J. Suppl.*, **2**, 389.
Hodapp, K.-W. 1984, *Astr. Ap.*, **141**, 255.
———. 1987, *Astr. Ap.*, **172**, 304.
Hodapp, K.-W., Capps, R. W., Strom. S. E., Salas, L., and Grasdalen, G. L. 1988, *Ap. J.*, **335**, 814.
Hodapp, K.-W., and Eiroa, C. 1989, *A.J.*, **97**, 166.
Hubble, E. P. 1916, *Ap. J.*, **44**, 190.
Hughes, V. A. 1988, *Ap. J.*, **333**, 788.
Jones, T. J., and Dyck, H. M. 1978, *Ap. J.*, **220**, 159.
Kaburaki, O., and Itoh, M. 1987, *Astr. Ap.*, **172**, 191.
Kobayashi, Y., Kawara, K., Maihara, T., Okuda, H., Sato, S., and Noguchi, K. 1978, *Pub. Astr. Soc. Japan*, **32**, 377.
Lenzen, R., Hodapp, K.-W., and Solf, J. 1984, *Astr. Ap.*, **137**, 202 (LHS).
Massi, M., Felli, M., and Simon, M. 1985, *Astr. Ap.*, **152**, 387.
Mathewson, D. S., and Ford, V. L., *Mem. R.A.S.*, **74**, 139.
Mathis, J. S., Mezger, P. G., and Panagia, N. 1983, *Astr. Ap.*, **128**, 212.
Moneti, A., Pipher, J. L., Helfer, H. L., McMillan, R. S., and Perry, M. L. 1984, *Ap. J.*, **282**, 508.
Mundt, R., and Fried, J. W. 1983, *Ap. J. (Letters)*, **274**, L83.
Nagata, T., Sato, S., and Kobayashi, Y. 1983, *Ap. J. (Letters)*, **119**, L1.
Pudritz, R. E., and Norman, C. A. 1986, *Ap. J.*, **301**, 571.
Röser, H.-J. 1981, *Astr. Ap.*, **103**, 374.
Sargent, A. I. 1977, *Ap. J.*, **218**, 736.
Schmidt, J. F. J. 1861, *Astr. Nach.*, **55**, 91.
Snell, R. L., Scoville, N. Z., Sanders, D. B., and Erickson, N. R. 1984, *Ap. J.*, **284**, 176.
Strom, K. M., Strom, S. E., Wolff, S. C., Morgan, J., and Wenz, M. 1986, *Ap. J. Suppl.*, **62**, 39.
Werner, M. W., Dinerstein, H. L., and Capps, R. W. 1983, *Ap. J. (Letters)*, **265**, L13.
Yamashita, T., Sato, S., Nagata, T., Gatley, I., Hayashi, S. S., and Fukui, Y. 1989, *Ap. J.*, **336**, 832.

Note added in proof.—New *I*-band frames obtained recently under very good seeing conditions show the *I* band image of GL 490 to be extended and elongated by $\sim 1''$ along a position angle of $-60°$, i.e., roughly perpendicular to the outflow axis. This morphology can be explained by CPM's scattering model and some contribution of scattering to the *I* band polarization is therefore likely. If there is a positional shift between the *I* band and *K* band images of GL 490, it is too small to be detected in the saturated *K* band image (Fig. 5). The conclusions about the *I* band polarization of neighboring stars presented in this paper are not altered by this finding. It is still highly likely that at near infrared wavelengths, longward of 1 μm, the polarization of GL 490 is predominantly caused by aligned grains and that the near-infrared image is dominated by direct light from the central star.

K.-W. HODAPP: Institute for Astronomy, 2680 Woodlawn Drive, Honolulu, HI 96822